Detection of highly transient electric fields following ultra-intense laser interaction with solid targets

M Borghesi

Department of Pure and Applied Physics, The Queen's University, Belfast

D H Campbell, M G Haines, A Schiavi, O Willi*

The Blackett Laboratory, Imperial College of Science, Technology and Medicine, London

A J Mackinnon

Lawrence Livermore National Laboratory, Livermore (CA, USA)

M Galimberti, L A Gizzi

IFAM-CNR, Pisa (Italy)

R J Clarke, S Hawkes

Central Laser Facility, CLRC Rutherford Appleton Laboratory, Chilton, Didcot, Oxon, OX11 0QX, UK

H Ruhl,

Max-Born-Insitut, Berlin (Germany)

Main contact email address: *m.borghesi@qub.ac.uk*

** present address: Institut für Laser-und-Plasmaphysik, Heinrich-Heine-Universität, Düsseldorf (Germany)*

Introduction

We present here the first application of laser-produced protons as a particle probe in high-density matter investigations. By using the recently developed proton imaging technique[1)] the first direct demonstration of highly transient electric fields following ultra-intense laser-pulse interaction with plasmas has been obtained. The possibility (previously unavailable) of measuring transient electric fields with high temporal resolution permits the investigation of a range of important phenomena related to the generation and transport of hot electron currents. These issues are of enormous topical interest in view of the development of Fast Ignitor driven Inertial Confinement Fusion. They can now be accessed with a completely different approach, which allows study of the electron current dynamics with an unprecedented resolution in a direct and simple way.

Experimental arrangement

The proton beams were produced by focusing a high-intensity pulse (typically 20 J in 1 picosecond, focused at an intensity of 10^{19} Wcm^{-2}) onto the surface of Al foils. The protons were emitted normal to the back surface of the target with small angular divergence (about 10°), cut-off energy of 10 MeV, temperature of ~ 1 MeV (obtained by fitting a Boltzmann exponential to the proton spectrum), from a source with diameter smaller than 10-15 µm.

According to the models, the protons are accelerated for a time of the order of the laser pulse duration, as confirmed by our experimental tests[1)]. This provides very high temporal resolution for our particle probe, allowing the detection of highly transient phenomena. It should be remembered here that proton beams produced with conventional accelerators have a duration of several nanoseconds at best.

The detector employed consisted of a stack of several layers of radiochromic film (RCF)[1)]. By employing this technique, we have detected the onset of electric fields in various target configurations[2)]. We will discuss here the detection of highly transient fields following the irradiation of a solid target with an ultraintense, picosecond laser pulse. The experimental arrangement for these measurements is shown in Figure 1.

Two 1µm, 1 ps pulses (CPA_1 and CPA_2) produced by the Vulcan laser were focused onto separate targets at an intensity of 10^{19} W/cm^2. The CPA_2 pulse was focused onto an Al foil to produce a beam of protons, while the CPA_1 pulse was focused onto solid targets. The delay between the two pulses could be varied optically. The angle between proton beam direction and CPA_1 propagation directions was approximately 75°. The distances involved were: 2 mm (Al foil to main target), and 2.7 cm (main target to detector). As explained in Reference 1, the proton probe is used in a point-projection imaging arrangement with the magnification determined by the ratio of detector-to-object and object-to-source distances. The advantages of using an RCF-based detector are also discussed in Reference 1.

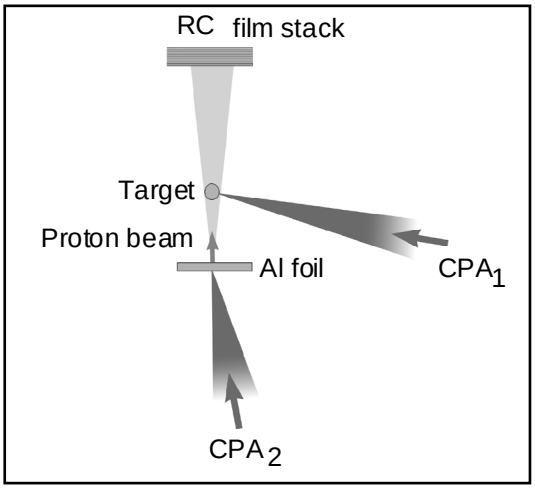

Figure 1. Experimental arrangement for proton probing of ultraintense laser-target interaction.

Experimental results

In Figure 2 proton images taken (in a single shot) after ultraintense irradiation of a 150 µm glass micro-balloon are shown. It can be seen (Figure 2(a)) that in coincidence with the interaction, a circular shadow, much larger than the projected target image, is observed in the detector. Here by shadow we mean a region of film unexposed to the proton flux. This shadow is consistent with protons that are deflected away from the target surface by an outwardly directed electric field. As a matter of fact, during the CPA_1 interaction, fast electrons are accelerated in the forward direction by the laser pulse in the interaction region at the front of the target. The energy of these electrons, in the MeV range, is large enough for them to reach the back of the target. Some of the electrons can actually escape from the target, before it charges up, preventing further loss of

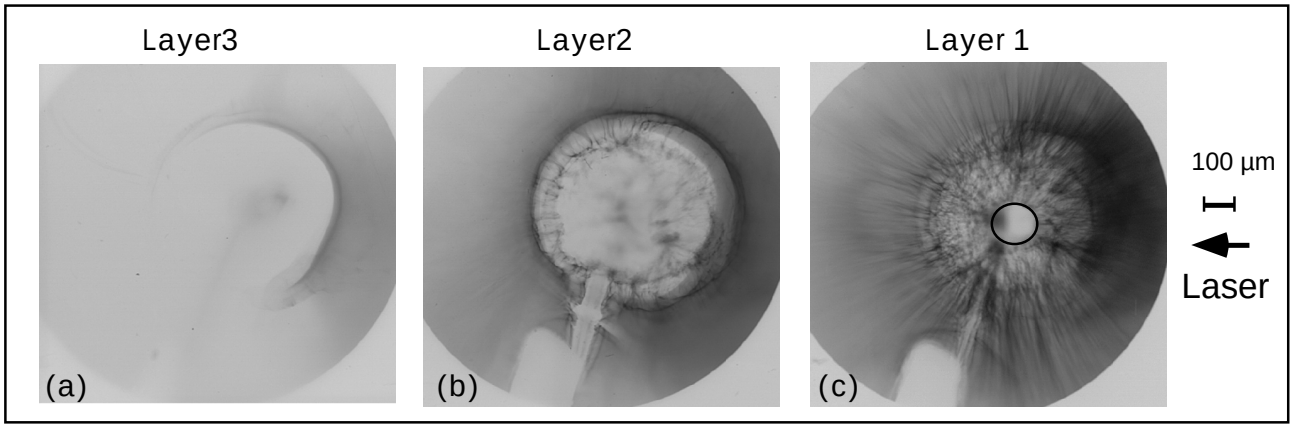

Figure 2. Proton images taken following CPA-irradiation of a 150 µm glass micro-balloon. The original size and position of the target are indicated by the black circle in (c). Each picture refers to subsequent RCF layers (i.e. different proton energy Ep and different probing delay Δt from the interaction): (a) Ep~ 8 MeV, Δt~ 0; (b) Ep~ 6-7 MeV, Δt~10 ps; (c) Ep~ 3-5 MeV, Δt~20-35 ps. The spatial scale indicated refers to the target plane: distances in the image plane are M times larger (M~13 is the geometric magnification).

electrons. The proton deflection we observe is due to this charge.

An analytical expression for the position in the image plane of a proton of the beam can be easily obtained, taking account of the deflection experienced by the proton in the Coulomb field of the charged sphere[3] :

$$x = d \tan\alpha + L \tan(\alpha + 2\tan^{-1}(Q/8\pi\varepsilon_0 V d \sin\alpha))$$

where V is the energy of the proton in eV, α is the angle formed by the proton with the beam propagation axis, ε_0 is the permittivity of vacuum and Q is the charge of the target (SI units). By supposing, for simplicity, uniform proton emission within a cone of aperture α_0, the proton density distribution in the detector plane can be calculated for an arbitrary Q.

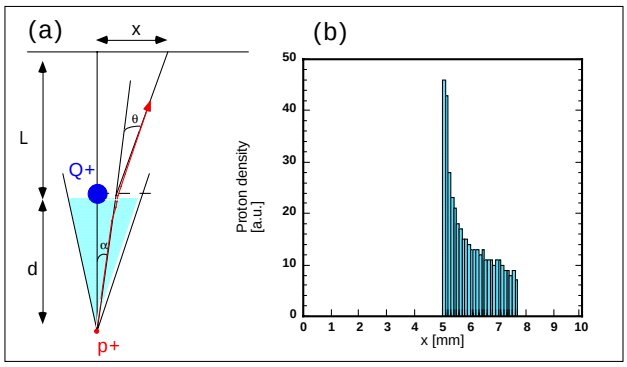

Figure 3. (a) Schematic of proton deflection in presence of a charge Q. (b) Calculated radial proton distribution at the detector plane (for V = 8 MeV, Q= 2.10^{-8} C), reproducing the experimental data of Figure 2(a).

The radial distribution shows a pronounced peak due to proton pile-up. Matching the peak position with the experimental one yields the value of Q (Figure 3). In this way, the charge at t = 0 was estimated to be Q ~ 2.10^{-8} C, corresponding to 10^{11} electrons leaving the target during the interaction.

As visible from Figure 2, a rapid discharge of the target was observed following the interaction. By applying the method described above to the different layers, and using data taken with different CPA_1-CPA_2 delays, the temporal evolution of the target's charge could be reconstructed, as shown in Figure 3. The charge decays exponentially, with a time constant of approximately 25 ps. We believe that the observation is consistent with the expelled electrons flowing back into the target. As a matter of fact, the electrons leaving the target will also move in the potential of the positively charged microballoon. They will reach a maximum distance from the target, after which they will be called back into the target. This is the most likely mechanism able to explain the discharge considering its short timescale.

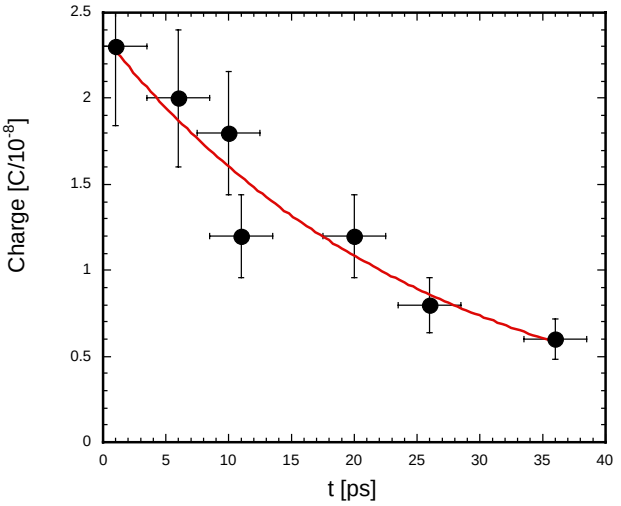

Figure 4. Temporal evolution of the charge of the laser-irradiated microballoon. The solid line represents an exponential fit of the data.

This assumption is supported by another phenomenon clearly visible in the data shown in Figure 2. Simultaneously with the discharge, the onset of filamentary structures at the target surface after the interaction was observed. The filamentary structures are first seen 10-20 ps after the interaction, and appear as striations extending outwards along the normal to the target surface, even far away from the interaction region. This is clear in Figure 2(b) where the filaments start to appear, and in Figure 2(c), where they have fully grown. In Figure 2(c) the filaments are seen both side-on and face-on (as a speckled pattern inside the shadow). The transverse wavelength of the modulation is about 10 µm and is more or less constant over the whole field of observation.

The observations are consistent with the growth, at the surface of the target, of an electromagnetic heat-flow instability[4], arising in presence of two counterstreaming currents. This takes place when the returning current of hot electrons flows back into the target, and draws an opposite current of cold electrons from the target in order to preserve charge neutrality. Filamentary structures similar to the ones of Figure 2 were observed via optical probing in long pulse experiments about 20 years ago[5]. However, optical probing could only detect density perturbations in the coronal plasma with limited

temporal resolution, and only speculations could be made on the origin and nature of the filaments in that experimental setting.

Heat-flow instabilities have been studied theoretically for a long time due to their potentially detrimental effect on compression in conventional Inertial Confinement Fusion (ICF), and, more recently, due to the renewed interest in fast electron transport associated with the Fast Ignitor Scheme for ICF. The electrothermal instability[6], which takes place in presence of counter-streaming flows of collisionless hot electrons and cold collisional electrons is particularly relevant to our experimental conditions. As the instability causes magnetized filamentation of both hot and cold currents, the effect is imprinted on the diagnostic proton beam via the associated electric fields, transverse to the filaments. The instability grows at the target surface and the perturbations are transported out by the expanding plasma. Essentially the magnetic fields are frozen into the ablating plasma. Reference 6 provides order of magnitude scaling laws (which are independent from the intensity of the hot electron flux) for the growth rate α and the transverse wavelength λ of the modulation, i.e. $\alpha[s^{-1}] = 2.8\cdot 10^{-8} n_0 Z / A T_e^{3/2}$, $\lambda[m] = 2.41\cdot 10^{10} T_e^2 \sqrt{A}/n_0 Z$. n_0 and T_e are density and temperature of the cold electrons, Z and A charge and atomic number of the target material. For example, by using the density of solid glass ($n_0 \sim 5.10^{28}$ m^{-3}), Z and A for Si (main constituent of the glass target) and T_e= 500 eV, one obtains $\alpha^{-1} \sim 15$ ps and $\lambda \sim 5$ µm, of the order of the observations. It should be noted that a 500 eV temperature is consistent with the upper bound imposed by the validity condition of the model (cold mean-free path less than collisionless skin depth). Once the magnetic field of the instability has grown sufficiently ($\Omega_0\tau_c$>1), the thermal conduction reduces, the condition no longer applies, but the filaments become frozen-in.

Features similar to the ones discussed up to now were observed during the interaction with a range of solid targets. Particularly dramatic effects were observed probing the interaction of the CPA_1 pulse with small diameter metal wires. Figure 5 shows proton images of the interaction with a 50 µm Ta wire. The RCF layers shown (second layers of the RCF stacks, corresponding to proton energies of 6-7 MeV) have been obtained in separate shots for different CPA_1-CPA_2 delays. When the proton probe arrived on target before the CPA_2 interaction pulse (e.g., t=-10 ps, 1st image in Figure 5), only the shadow of the Ta wire, thick enough to slow down the protons is visible, with some small effect visible in the interaction region due to preplasma present ahead of the interaction. However when the probe is incident with the interaction a dramatic effect is observed, with the protons being deflected away from the wire surface, which again charges up due to hot electron expulsion. Even in this case the charge is seen to decay in a few tens of picoseconds, and filamentary structures are seen to appear. In this case the onset of pronounced horizontal features above and below the interaction axis is also detected. This data is still being analysed. However we think this structure may be related to the radial expansion of shocks following the interaction, likely presenting non-neutral regions at their leading front. The complex pattern observed with RCF was reproduced when CR39, a nuclear track detector was used. The data of Figure 6 was obtained with a layer of CR39 film placed immediately behind one of the RCF layers shown in Figure 5 (the third from the left). Allowing for the time difference and the lower spatial resolution of CR39, the features are all reproduced, providing further confirmation that all the features observed are due to protons within the estimated energy range.

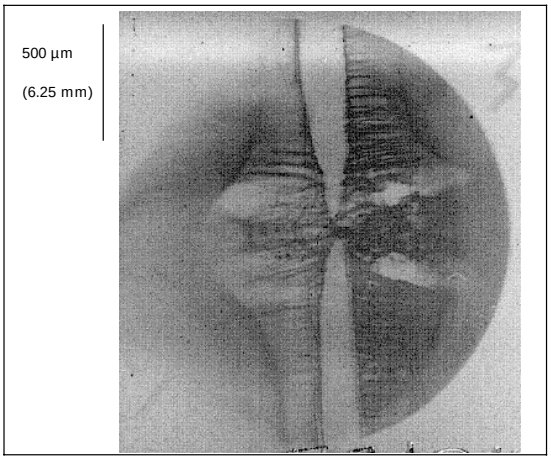

Figure 6. Proton image obtained with CR39 (8MeV protons). The detector was placed immediately after the central layer of Figure 5.

Conclusion

Proton imaging has enormous potential for the diagnosis of fundamental physical problems, which were impossible to explore up to now. By using this diagnostic, for the first time the measurement of very large, highly transient electric fields in plasmas has been obtained, determining their evolution on a picosecond scale with micrometric spatial resolution. In particular, global charge-up of a microscopic target irradiated by a high-intensity laser has been observed for the first time.

References

1. M.Borghesi *et al*, in this Annual report
2. M.Borghesi *et al;* A.Schiavi *et al*, in this Annual report
3. O.Klemperer , Electron physics, Butterworths, London (1972)
4. M H Key ,Compression and hydrodynamics, in Laser-plasma Interactions 3, SUSSP 29 (1985)
5. O Willi *et al*, Opt. Comm., 41, 110 (1982)
6. M Haines, Phys. Rev. Lett., 47, 918 (1981)

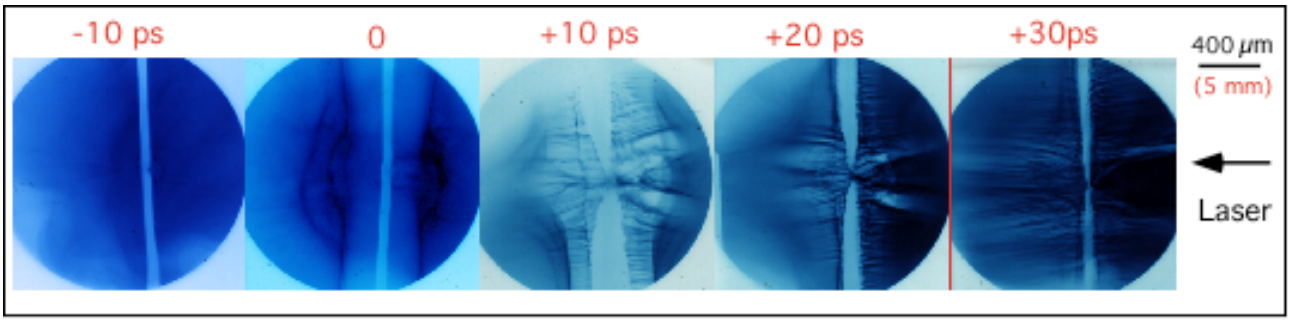

Figure 5. Temporal evolution of proton images of the interaction zone for different interaction-probing delays. The target was a 50 µm Ta wire and the energy of the protons employed was 6-7 MeV. The delay between CPA_1 interaction and probing is indicated above each of the pictures. Spatial scales for both the target and the image plane (between bracket) are indicated.